Technical Paper

ISSN 1997-1400 Int. J. Pavement Res. and Technol. 1(4):148-154

Analysis of Slab Thermal Stresses and Concrete Joint Movements

Chia-pei Chou[1] and Mei-hui Lee[2+]

Abstract: A field experiment project was conducted at the Taiwan Taoyuan International Airport during slab replacement maintenance. Thermal sensors and optical fiber sensors were installed in four concrete slabs. The main objective of this paper is to analyze the variation of slab curling stresses during a day as well as during a year. In addition, measurements from fiber sensors can be used to calculate the joint movement along with the seasonal changes. The analysis of slab thermal stress included long term seasonal stress and delay warping curing stress. The induced crack occurred four days after the joint saw cut, and the initial crack width was about 0.29*mm*. Concrete slabs shrink during the curing stage, mainly due to drying shrinkage. Joint movement became more sensitive to air temperature approximately two weeks after curing. The slab moved toward the joint when the air temperature increased from January to June and away from the joint to its center line from September to January. The measured average moving rate was 0.035*mm* per Celsius degree for a 7*m* slab. Partially restrained thermal stresses were estimated based on further analyses of measured thermal strains in the instrumented slab. The study found that the actual (partially restrained) thermal stress at the top of the slab was much lower than the theoretical value, which is based on the assumption that the slab is completely restrained. The actual thermal stress at the slab bottom, however, was rather close to the theoretic stress. This discrepancy is mainly due to the high restriction of movement at the slab bottom.

Key words: *Curling stress; Fiber sensors; Joint movement; Rigid pavement; Thermal stress.*

Background

The Taiwan Taoyuan International Airport (TTI Airport) is the busiest and most important international airport in Taiwan. It was first opened to commercial air traffic in 1979 with one 3,660*m* runway. A second runway, approximately parallel to the first one, became operational in 1984. Based on data collected in 2002, the TTI Airport runs 123,900 operations and serves 18.5 million passengers annually. In the airport, the annual mean temperature is 23.5℃ and the annual mean relative humidity is 74%.

The airside of TTI Airport is constructed with jointed plain concrete pavement. Due to extensive use of the airport for the past twenty years, many concrete slabs have deteriorated badly. Starting from 2000, numerous concrete slabs on the runways and taxiways and on the apron have been repaired by partial depth patches or full depth patches, with the worst ones being replaced. Later, it was discovered that some of the replaced slabs were again damaged not long after their replacement. A rigorous examination of airport pavement behavior is thus vital to the understanding of the impact of aircraft traffic and of the environment on pavement performance.

In January 2002, a total of 102 static and dynamic sensors were embedded in the concrete slabs on taxiway N1 at the TTI Airport. Taxiway N1 is the primary taxiway, serving 42% of the departure aircraft and 18% of the arriving aircraft. These figures translate into approximately 26,000 and 11,100 annual operations, respectively. The static sensors include 14 temperature sensors, three moisture sensors, and seven optical fiber sensors. Their dynamic counterparts consist of 20 position sensors, 42 H-bar stain sensors, and 16 dowel bar strain sensors.

Related Research

Each country has been conducting many rigid pavement monitoring programs for years to observe the reactions of rigid pavement under the effects of environmental factors and loading. Furthermore, the reactions to the aspects of designing, analyzing, and evaluation methods were applied. The American Engineering Corps started their research on the designing methods of rigid pavement during World War II, and their on-the-spot experimental results tested and verified Westergaard's edge loading analysis model [1]. A set of joint load transfer model was then developed to provide principles of joint design and pavement designing methods with more conforming to economical benefits. However, their experiment failed to find out the effects on pavement achievements caused by temperature and humidity, and methods of improvement were not obtained either. Rollings and Witczak [2] used full scale acceleration experimental results of American Engineering Corps to analyze and then developed Structural Condition Index to evaluate structural benefits of the pavement. But that model only took destruction caused by fatigue loading into consideration. There are still many destruction forms being eliminated and they had to be evaluated separately.

The Federal Aviation Administration's (FAA) Airport Technology Research and Development Branch has been conducting research concerning airport pavement for years. Several projects examined rigid pavement, including the Airport Pavement Instrumentation Project at the Denver International Airport and National Airport Pavement Test Facility (NAPTF). Kapiri et al. [3] used the live data

[1] Department of Civil Engineering, National Taiwan University, No.1, Sec.4, Roosevelt Rd., Taipei 106, Taiwan.
[2] Department of Civil Engineering, National Taiwan University, No.1, Sec.4, Roosevelt Rd., Taipei 106, Taiwan.
[+] Corresponding Author: E-mail f91521511@ntu.edu.tw
Note: Submitted March 18, 2008; Revised June 5, 2008; Accepted June 19, 2008.

from Denver Airport and compared them with simulated data from the Industrial-Construction Management (ICM) 2.0 program. From historical data and application of ICM, we found the joint's load transfer efficiency (LTE) on the slab in different seasons.

Hayhoe et al. [4] used the data from NAPTF to analyze the interaction among plane wheels, the track gauge, and the pavement. They compared the interaction differences between dead loading and dynamic loading and also the differences between live experimental values and data analytical values. The Engineering and Research International (ERI) was entrusted by the FAA to conduct an experiment with Konsult and Utveckling AB (Kuab) 2*m* Heavy Weight Deflectometer (HWD) at NAPTF. From the analysis, they realized that the back-calculation data of HWD was not only related to the material quality, but also closely related to the structural model and the boundary condition. They discovered that the joint load transfer effects were affected by the dynamic loading movement direction and that the transverse joint was more affected by load transfer direction [5]. In 2000, NAPTF examined three different types of pavement to conduct an experiment using a four-wheeled or six-wheeled machine with each wheel weighing 20.4tons (45,000lbs). They applied the data collected from the strain gage to differentiate the strain condition of the plate when a corner crack occurred because they discovered that the plate caused corner crack at the beginning of the experiment [6].

There are still many other programs that monitor how the plate changes as the environmental temperature varies. The National Expressway Engineering Bureau of the Ministry of Transportation and Communications in Taiwan Area set up underground monitoring equipment on the second highway from section 57k+344.2 to 57k+377.8 in 1993, and they also established a Weigh-in-Motion to measure the carrying capacity of passing vehicles. They developed a program which simulated temperature stress and curling deformation. The results of the simulation showed that curling stress was the greatest at 4:00 in the afternoon and that temperature stress was greater than the stress produced by carrying capacity [7]. In 1994, Lee [8] carried out an experiment to monitor the experimental plate at TTI airport. The results showed that air voids had a greater effect on the coefficient of thermal diffusivity than the aggregate quantity contained to dry concrete. He also discovered that the coefficient of thermal expansion calculated with the coefficient of thermal diffusivity measured by concrete which agreed with thermal resistance series connection theory, simulated the effects of temperature changes more effectively; the water to cement ratio in the concrete had a great impact on the coefficient of thermal diffusivity.

Mohamed and Hansen [9] developed a set of methods to calculate the remaining stress produced by a nonlinear stress strain gradient along the depth of the plate. They compared between the nonlinear temperature gradient inferred from the live data and the calculated results of the traditional hypothetical linear temperature gradient. The two calculated results assumed by these temperature gradients had great differences in the early morning and at night. The linear hypothesis underestimated tensile stress produced by the bottom of plate. Ramadhan and Al-abdul Wahhab [10] carried out two experiments to observe the conditions of asphalt and rigid pavement at King Fahd University of Petroleum and Minerals in the east province of Saudi Arabia under changing temperatures. They applied the experimental statistics to establish a temperature database, develop a temperature forecast equation for asphalt pavement, and observe the temperature gradient along the depth in the rigid pavement.

In 1999, Balbo and Severi [11] conducted an experiment to monitor plate temperature at Sao Paulo University. The experiment provided experimental statistics of the temperature distribution in a concrete plate in a tropical climate. They discovered that under hot and humid conditions, the positive temperature difference was longer than the negative one: about 75% of a single day had a positive temperature difference, and the difference could be up to 25 ℃. About 90% of the temperature distribution along the depth of the plate was nonlinear, and among them two times was distributed most. In spring and summer, the day time temperature gradient was 0.65~0.82℃/*cm*, but the gravel bottom layer was saturated, then the day time temperature gradient would climb up to 1.33℃/*cm*.

In the same year, Beckemeyer et al. [12] conducted an experiment on America's I-80 highway to research the behavioral differences of a joint rigid concrete surface on two different bottom layers oil/grit separators and asphalt treated permeable base (OGS and ATPB). The results showed that the main factors affected inner curling were (1) the temperature gradient in the plate when the concrete hardened, (2) divergent shrinkage, (3) the thermal parameter of the concrete, and (4) methods utilized to maintain the plate. Under the influence of built-in curling, curling did not necessarily occur when the temperature gradient was zero. The main factor resulting in top-down cracking was built-in slab curling. From the view of fatigue analysis, they discovered that if the joint space was reduced to 4.57m (15*ft*) or less, then the chances that top-down fissures occurred would be greatly reduced.

Sensors Layout

Temperature sensors were placed at different depths in the concrete slab. A set of seven sensors were vertically embedded at the center of the 7 by 6*m* slab, while a parallel set of seven sensors was placed near the edge of the same slab at similar vertical locations (Fig. 1). Temperature data were recorded at two-minute intervals to provide adequate pavement temperature readings under different weather conditions; for example, afternoon thunderstorms are frequent during the summer, and they can cause the pavement temperature to fluctuate dramatically.

Optical fiber sensors were lined up in the longitudinal direction in the middle of concrete slabs. Each Surveillance des Ouvrages par Fibres Optiques (SOFO) optical fiber sensor is loosely tied to the rebar racks that are designed to support the sensors. Sensor 1 begins at the center point of slab #6 and ends at slab #7. Sensors are lined up with a 5*cm* gap between them, so the total length of the first six sensors is around 325*cm*. The function of each sensor is to measure the total movement of concrete for the specified 50*cm* except the 7th sensor. Sensor 7 is across the joint of slab #6 and slab #7, and about 16*cm* down from the slab surface. The major function of sensor 7 is to measure the joint movement between these two slabs (Fig. 1).

The first set of sensor readings started at noon on January 3, 2002, right before concrete was poured. All seven sensors were reset to zero at the concrete pouring time. Therefore, the reading of sensors 1 to 6 thereafter represent the concrete movements within each

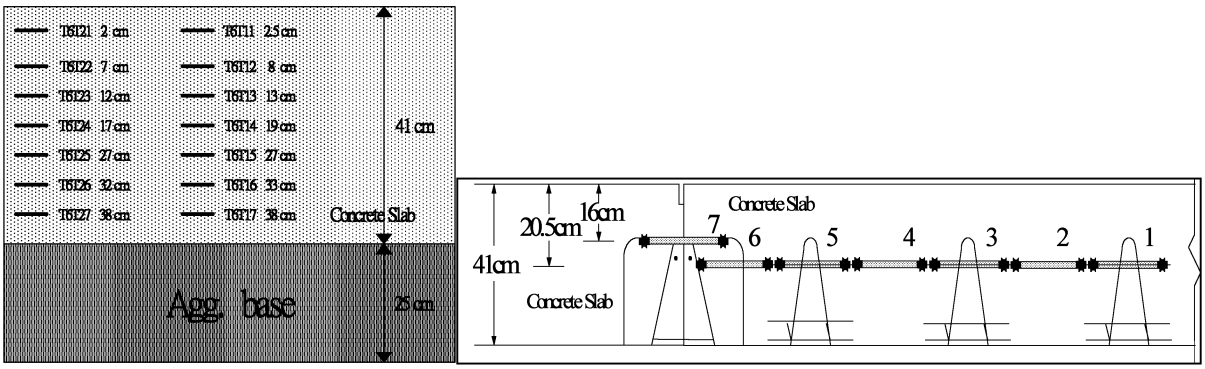

Fig. 1. Layout of Thermal and Fiber Sensors in the Experimental Concrete Slab Field.

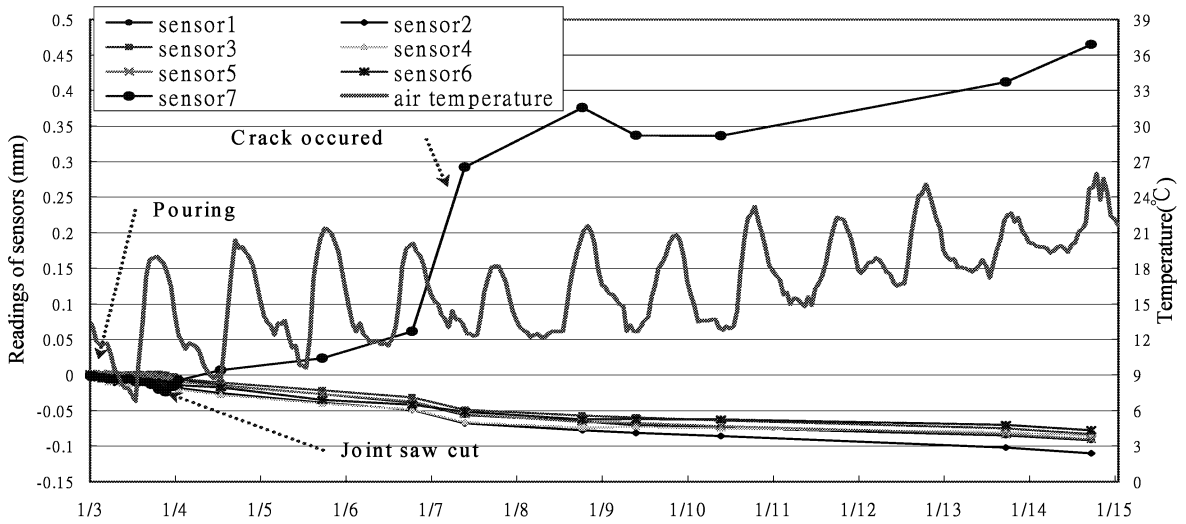

Fig. 2. Readings of Sensors and Air Temperatures for the First Thirteen Days of Concrete Slab Curing.

specified 50*cm*, and the reading of sensor 7 (L_{S7}) represents the joint movement. Data were collected at 20 minute intervals during the concrete pouring process. All sensors are relatively stable at the pouring time, but started to shrink when the concrete entered the curing process. Once the slab was sawn, sensor 7 expanded and the other six sensors kept shrinking toward to the slab center at an even greater speed. Fig. 2 displays the seven sensor readings and the air temperature for the first 13 days, January 3 to January 15, 2002. It is clear that sensor 7 elongates from the time of sawing when slabs #6 and #7 move oppositely toward each slab's center. Since sensor 7 is across slabs #6 and #7, this elongation represents the volume of joint movements at the joint from both half slabs, assuming that each slab moves symmetrically with respect to its center line (Fig. 1). Although the daily temperature cycles up and down with its highest temperature increasing gradually between January 4 and 6, Fig. 2 illustrates that the concrete slab continues shrinking during this time period. This indicates the movement is more sensitive to concrete drying shrinkage than air temperature variations. Sensor 7 expanded from a negative value (-0.013*mm*) to a positive value of 0.065*mm* at noon on January 7. However, slabs #6 and #7 were still in the continuous form at the depth of sensor 7, since movement of 0.065*mm* is too small to be the crack width, even in its initial stage. A big jump in value, from 0.065 to 0.292*mm*, was found between January 7 and 8. Those days also had a large increase in air temperature. It is assumed that the crack induced by the saw cut went through sensor 7 during this time period, and the initial crack width was determined to be close to 0.29*mm*. Readings from 0.29 to 0.44*mm* were recorded from January 8 to 15. It is observed that the readings of sensor 7 are affected more by air temperature during this time period than before. The data provide a great picture of the concrete slab behavior during its first curing stage.

Slab Temperature Analysis

Figs. 3(a) and 3(b) illustrate the temperature distribution in the center of slab #6 in different seasons. In summer, the temperature at the top of slab is always higher than air temperature at any time, but it becomes the same as the air temperature during the nighttime of winter. It is concluded that the slab absorbs less heat energy in winter, and therefore the heat disperses easily during the night. Fig. 4 displays the slab temperature distribution when it rains. The temperature at the top of slab is lower than that at the bottom, and it shows a negative temperature difference in that period.

Fig. 5 is a typical diagram displaying the nonlinear temperature differentials of concrete slabs at one-hour intervals in a given day. In this figure, the temperature of the bottom sensor is used as the base for measuring the performance of the other six sensors. The positive temperature differential of concrete slab lasts about 12 hours, from 9 a.m. to 9p.m. The maximum temperature gradient (0.031°C/*mm* (1.42°F/*inch*)) occurs in the early afternoon (2p.m.) and is roughly

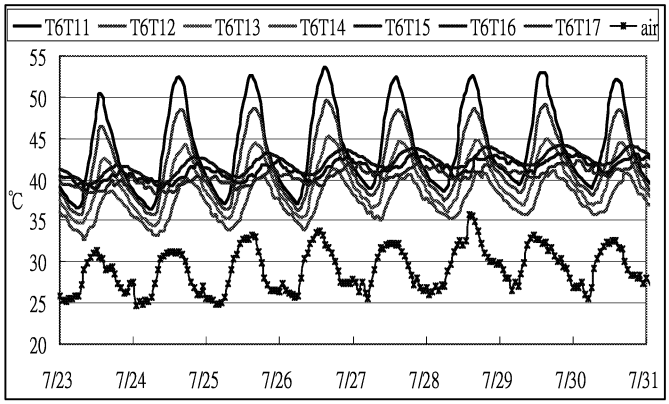

(a)

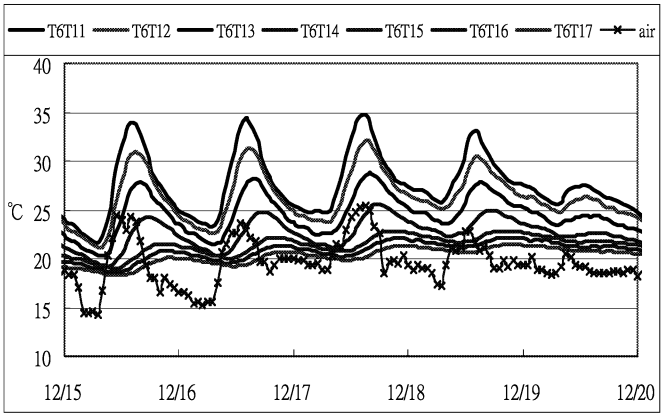

(b)

Fig. 3. Slab and Air Temperature Distribution in (a) Summer and (b) Winter.

three times the value of the maximum negative temperature gradient, which is about 0.011°C/*mm* (0.50°F/*inch*) measured in the early morning (5a.m.). The temperature curve of the top four sensors shows a "wave shape" within the positive temperature gradient domain and descends smoothly into a more linear shape within the negative temperature gradient domain.

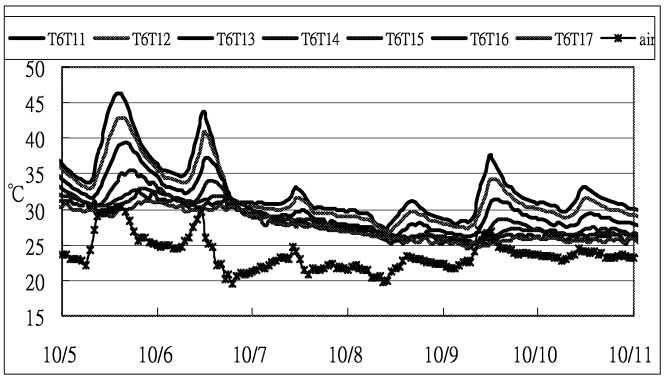

Fig. 4. Slab and Air Temperature Distribution on a Rainy Day.

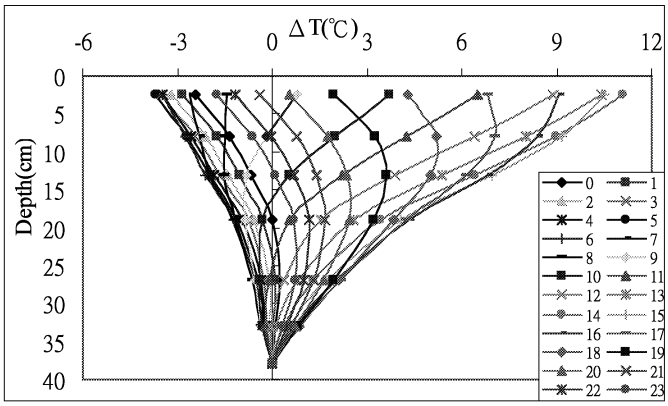

Fig. 5. Temperature Differentials by Depth at One Hour Intervals during the Course of a Day.

Joint Movement along with Seasonal Temperature Variations

From either theoretical analysis or field observations, it is known that a concrete slab moves toward its center when the temperature drops, and expands to the joint under high temperature conditions. Data collected from the TTI airport experimental field fully coincide

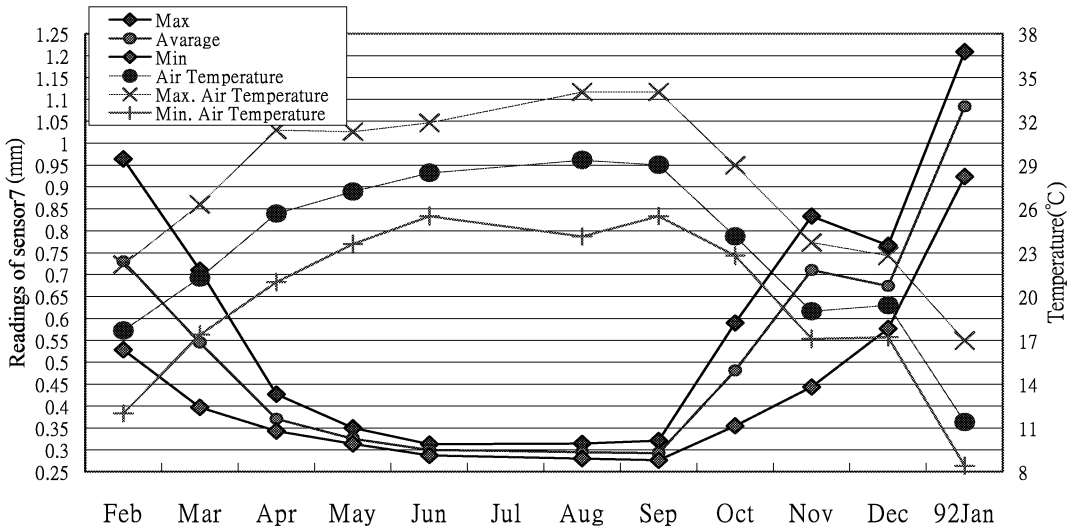

Fig. 6. Monthly Maximum, Minimum, and Average Readings of Sensor 7 with Air Temperatures.

with these phenomena. However, the self weight of a concrete slab and the friction force between the slab and the sub-base layer also give great resistance to the horizontal movement of slab. The fiber optic field data was collected continuously 48 hours per month on a monthly basis. Fig. 6 is the plot the readings of sensor 7 from December 2002 to January 2003. It noted that the readings of sensor shows the test results of two modified asphalt binders of PG76 and 7 decrease gradually from 0.964*mm* (Feb. 2002) to 0.287*mm* (June 2002) with the increase in air temperature. The average decreasing rate is 0.034*mm* per °C. However, sensor 7 reaches its shortest length in September. The decreasing rate significantly slows down from June to September, with an average decreasing rate of 0.005*mm* per °C of air temperature increase. The decreasing rate of sensor 7 in the hot seasons is much less than that in the cool seasons, due to the limited space for slabs expansion. This is mainly because the concrete slabs were constructed and sawn in January, a relatively low temperature season. The slabs were at their shortest condition during that time. The joint saw cut only reaches the top one-fourth of the depth of slab; therefore, the gap at the middle joint depth was mainly created by the initial crack width plus slab shrinkage during the curing stage. This gap is usually not wide enough for slabs to expand on hot days. From Fig. 6 it is observed that the joint gap is almost closed between June to September, while readings of sensor 7 are around 0.28 ±0.01*mm*. These readings of sensor 7 coincide with the initial crack width measured at the crack occurrence as mentioned earlier in this paper. Since there is not enough space for the slab to expand between June and September, it is expected that the slabs have large compressive stresses during these months.

If we divide the elongation rate by the slab length, i.e., 7,000*mm*, we can obtain the real (partially restrained) expansion/shrinkage rate as (0.035*mm*/℃)/(7000*mm*) = 5 × 10^{-6}/℃(2.8 × 10^{-6}/°F), which is about half of the thermal coefficient of a concrete slab with gravel as the aggregate type (α=10 × 10^{-6}/℃). The American Association of State Highway and Transportation Officials (AASHTO) guide [13] adopted Darter's studies to determine the theoretical horizontal movements of a newly constructed rigid pavement, which is shown in Eq. (1) [14]. The adjustment factor C in this case is then calculated as (5 × 10^{-6}/10 × 10^{-6}) = 0.5.

$$\Delta L = CL(\alpha \times \Delta T + \varepsilon) \quad (1)$$

where ΔL: joint opening of the rigid pavement, *mm*; C: the adjustment factor due to the sub-base/slab friction restraint. 0.65 is used for the stabilized sub-base, and 0.80 is used for the granular base; L: slab length, *mm*; α: concrete thermal coefficient, 10 × 10^{-6}/℃(5.5 × 10^{-6}/°F); ΔT: temperature change (℃); and ε: the drying shrinkage coefficient of the rigid pavement.

Slab Thermal Stress Analysis

In this study, temperature stresses at different times of a day are calculated based on the slab temperature differentials and the measured slab strains. However, the creep and shrinkage of concrete are not considered in this research. If a slab is free to move and has a positive temperature differential, the top of the slab will expand by a strain of $\alpha_t \Delta t$ /2, and the bottom will contract by the same strain. The theoretical maximum stresses in the x- and y-directions at both top and bottom due to the completely restrained thermal strain for a finite slab can be determined. The reality is that the slab is partially restrained with only certain allowable movements in both the x- and y- directions. In this study, these movements are measured by H-bar strain gauges at the slab center. ε_x and ε_y are set as the theoretical strains under the zero restraint condition; ε_x' and ε_y' are the measured strain in the x- and y-directions, respectively. The actual

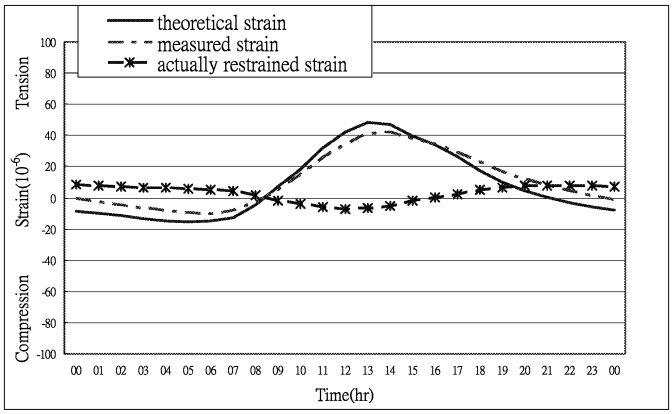

(a)

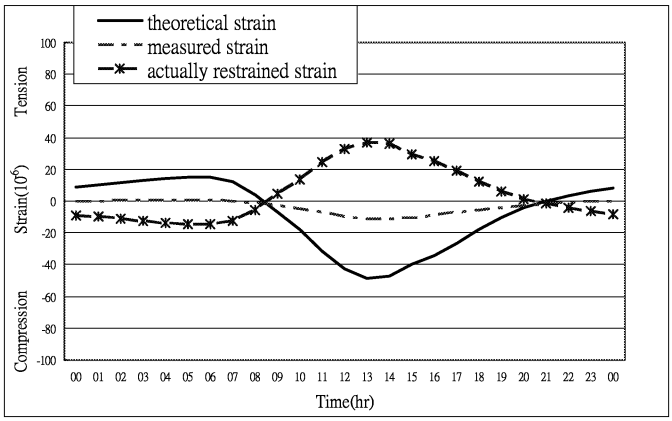

(b)

Fig. 7. Theoretical, Measured, and Derived Restrained Strains at the (a) Top and (b) Bottom of the Slab.

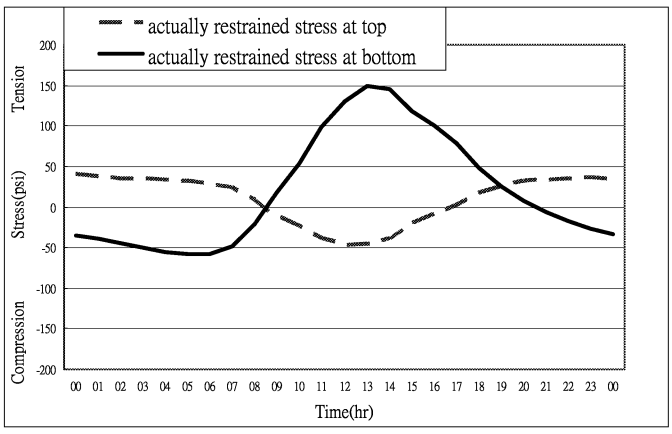

Fig. 8. Restrained Thermal Stresses Calculated over the Course of a Day at the Top and Bottom of the Interior of Slab.

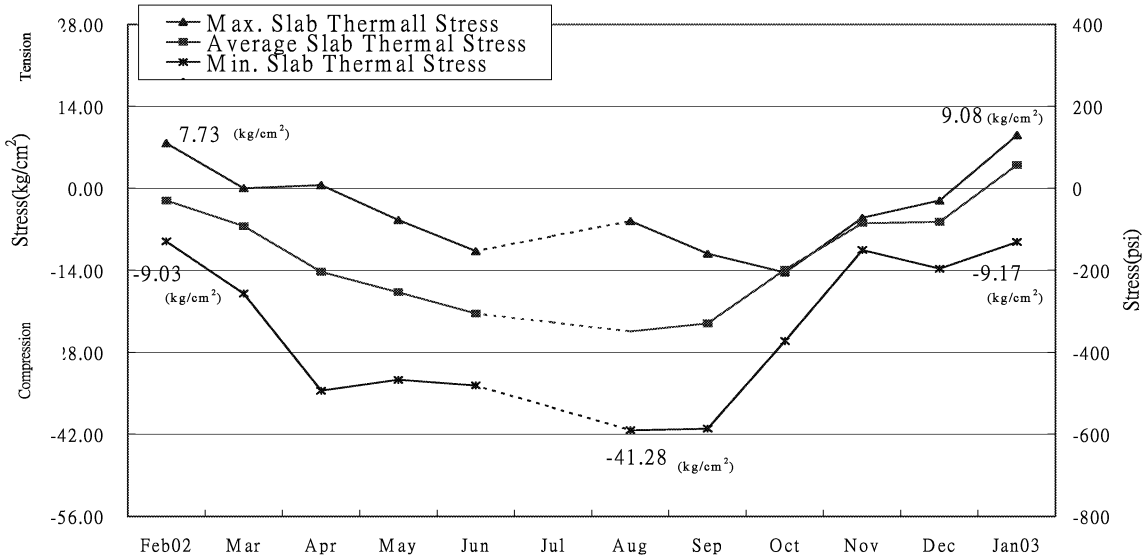

Fig. 9. Maximum, Minimum, and Average Concrete Slab Thermal Stresses from February 2002 to January 2003.

(partially restrained) thermal strains, ε_x" and ε_y" are obtained by Eqs. (2) and (3).

$$\varepsilon'_x \varepsilon_x = \varepsilon''_x \tag{2}$$

$$\varepsilon'_y \varepsilon_y = \varepsilon''_y \tag{3}$$

Figs. 7(a) and 7(b) provide the theoretical (ε_y), measured (ε_y'), and actual restrained (ε_y") stresses of the interior of the slab in the *y*-direction, both at the top and at the bottom, respectively. Fig. 8 displays the restrained thermal stresses of the instrumented slab at both top and bottom locations during the day calculated based on ε_x" and ε_y". The study finds that the bottom of the slab sustains tension from 8:30a.m. to 8p.m., with a maximum tensile stress of around 10.5*kg/cm*^{2} (150*psi*), which is much greater than the stress buildup during the hours of compression. The top of the slab is, on the contrary, in compression during the daytime from 8 a.m. until 5 p.m., and the maximum tensile stress is only 3.5*kg/cm*^{2} (50*psi*), which is much lower than the bottom stress.

Furthermore, the theoretical analysis of slab thermal stresses due to temperature variations can be calculated: if the slab is under completely free conditions ($C = 1$) and concrete moisture shrinkage is considered separately, the joint movements in Eq. (1) can be computed as $\Delta L_T = L\ (\alpha \times \Delta T)$. However, actual joint movement, ΔL, is different from the theoretical joint movement, ΔL_T, because of the partially restrained condition. Thus, the restrained strain is calculated as $((\Delta L_T - L)/L)$, and restrained stress can be computed by Eq. (4).

$$\sigma = ((\Delta L_T - \Delta L)/L) \times E \tag{4}$$

where ΔL_T: theoretical joint movement due to temperature change, *mm*; ΔL: actual joint movements, *mm*; *L*: slab length, *m* (*in*); *E*: Young's modulus, *kg/cm*^{2} (*psi*); α:concrete thermal coefficient; and σ: thermal stresses of concrete slab due to the temperature variations under the partially restrained condition (negative value as compression and positive value for tension), *kg/cm*^{2} (*lb/ in*^{2}).

In this study, it is assumed that α is around 10×10^{-6}/°C (5.5×10^{-6}/°F) for concrete with gravel aggregates. However, if we use the measured joint movement, L_{S7}, to compute the actual horizontal strain of concrete slab as in Eq. (5), the critical thermal stresses that occur at the maximum temperature variations can be obtained.

$$\sigma = ((\alpha \times \Delta T) - L_{S7}/L) \times E \tag{5}$$

where ΔT: the temperature difference between the time of placement to the time at analyzing point, °C (°F) and σ, α, ΔT, L_{S7}, *L*, and *E* are defined as above.

For the computed result, compressive stress should occur at the interior slab while tensile stress occurs at the both ends. Fig. 9 displays the computed maximum, minimum, and average slab thermal stresses from February, 2002 to January, 2003. The calculated result might be treated as the possibly extreme value of thermal stress that may occur in this specific test field. It is important to note that the thermal stress of experimental concrete slabs are in compression at most times during the year, since concrete material has a rather high compressive strength; for example the compressive strength was 455*kg/cm*^{2} (6500*psi*) at 28 days in this study, comparing with its tensile strength. The maximum compressive stress occurs in September, and the value is 41*kg/cm*^{2} (586*psi*).

It is also noted that the slab has tensile stresses in cold days, but the value is relatively low, 9*kg/cm*^{2} (130*psi*), comparing with its tensile strength, 49*kg/cm*^{2} (710*psi*). However, thermal stresses of concrete slabs will be in tension most of the time if concrete slabs are constructed on a hot day. It is always considered as a better-construction plan if the concrete construction can be scheduled during seasons with relatively low temperatures.

Conclusions

The following conclusions are drawn:

1. Concrete shrinks immediately after it is poured, and the shrinking speed is even faster after a joint saw cut. The

induced crack does not occur until four days later in this study, and the initial crack width was measured as 0.29*mm*. At the early stage of curing, drying shrinkage dominates the joint movements.

2. Slab temperature, especially on the surface, is greatly affected by the air temperature. However, the temperature on the interior of the slab is subject to changes of the surface temperature plus a time-delay factor.
3. Temperature variation at the top of the slab is much greater than that at the bottom. This results in a relatively larger movement at the top than at the bottom, and also coincides with the measurement of thermal strains at the slab interior.
4. The thermal stress under real conditions, partially restrained, is computed for the experimental slab. This study finds that the top thermal stress has a maximum tensile stress of $3.5 kg/cm^2$ ($50 psi$), while the bottom thermal stress experiences a maximum tensile stress of $10.5 kg/cm^2$ ($150 psi$). The latter value should be added to the wheel load stress for slab fatigue analysis.

References

1. Rollings, R.S. and Pittman, D.W., (1992). Field Instrumentation and Performance Monitoring of Rigid Pavements, *Journal of Transportation Engineering*, 118(3), pp. 361-370.
2. Rollings, R.S. and Witczak, M.W., (1990). Structural Deterioration Model for Rigid Airfield Pavement, *Journal of Transportation Engineering*, 116(4), pp. 479-491.
3. Kapiri, M., Tutumluer, E., and Barenberg, E.J., (2000). Analysis of Temperature Effects on Pavement Response at Denver International Airport, *Proceedings: International Air Transportation Conference*, San Francisco, California, USA, June, pp. 125-143.
4. Hayhoe, G.F., Cornwell, R., and Garg, N., (2001). Slow Rolling Responses Tests on the Test Pavements at the National Airport Pavement Test Facility (NAPTF), *Advancing Airfield Pavements: Proceedings of the 2001 Airfield Pavement Specialty Conference*, Chicago, Illinois, USA, Aug., pp. 30-58.
5. Guo, E.H. and Marsey, W., (2001). Verification of Curling in PCC Slabs at FAA National Pavement Test Facility, *Advancing Airfield Pavements: Proceedings of the 2001 Airfield Pavement Specialty Conference*, Chicago, Illinois, USA, Aug., pp. 15-29.
6. Guo, E.H., Hayhoe, G.F., and Brill, D.R., (2002). Analysis of NAPTF Traffic Test Data for First-Year Rigid Pavement Test Items, *the 2002 FAA Airport Technology Transfer Conference*, Atlantic City, New Jersey, USA, May, P-22.
7. Yan, C., (1992). Rigid Pavement Design Using Local Data, *research report*, Ministry of Transportation and Communications Taiwan Area National Expressway Engineering Bureau, Taiwan.
8. Lee, C.S., (1994). Monitoring and Analysis of Airport Rigid Pavement Under Thermal and Loading Conditions, *master thesis*, National Central University Department Civil Engineering, Taiwan.
9. Mohamed, A.R. and Hansen, W., (1996). Prediction of Stresses in Concrete Pavements Subjected to Non-linear Gradients, *Cement and Concrete Composites*, 18(6), pp. 381-387.
10. Ramadhan, R.H. and Al-abdul Wahhab, H.I., (1997). Temperature Variation of Flexible and Rigid Pavements in Eastern Saudi Arabia, *Building and Environment*, 32(4), pp. 367-373.
11. Balbo, J. and Severi, A., (2002). Thermal Gradients in Concrete Pavements in Tropical Environment: Experimental Appraisal, *Transportation Research Records*, No. 1809, pp. 12-22.
12. Beckemeyer, C.A., Khazanovich, L., and Thomas, H., (2002). Determination the Amount of Built-In Curling in JPCP: A Case Study of Pennsylvania I-80, *Transportation Research Records*, No. 1809, pp. 85-92.
13. American Association of State Highway and Transportation Officials, 「AASHTO, Guide for Design of Pavement Structures」, 1986.
14. Darter, M. I. (1977). Design of Zero-Maintenance Plain Jointed Concrete Pavement, Volume I-Development of Design Procedures, *FHWA-RD-77-111*, Federal Highway Administration, USA.